

# Is the Young Star RZ Piscium Consuming Its Own (Planetary) Offspring?

K. M. Punzi<sup>1</sup>, J. H. Kastner<sup>1</sup>, C. Melis<sup>2</sup>, B. Zuckerman<sup>3</sup>, C. Pilachowski<sup>4</sup>, L.  
Gingerich<sup>1,5</sup>, T. Knapp<sup>1,6</sup>

Received \_\_\_\_\_; accepted \_\_\_\_\_

---

<sup>1</sup>Center for Imaging Science, School of Physics & Astronomy, and Laboratory for Multiwavelength Astrophysics, Rochester Institute of Technology, 74 Lomb Memorial Drive, Rochester NY 14623, USA

<sup>2</sup>University of California, San Diego, 9500 Gilman Drive, La Jolla, CA 92093, USA

<sup>3</sup>University of California, Los Angeles, CA 90095, USA

<sup>4</sup>Indiana University, 107 S. Indiana Avenue, Bloomington, IN 47405-7000, USA

<sup>5</sup>Haverford College, 370 Lancaster Avenue, Haverford, PA 19041, USA

<sup>6</sup>Ithaca College, 953 Danby Road, Ithaca, NY 14850, USA

## ABSTRACT

The erratically variable star RZ Piscium (RZ Psc) displays extreme optical dropout events and strikingly large excess infrared emission. To ascertain the evolutionary status of this intriguing star, we obtained observations of RZ Psc with the European Space Agency’s *X-ray Multi-Mirror Mission (XMM-Newton)*, as well as high-resolution optical spectroscopy with the Hamilton Echelle on the Lick Shane 3 m telescope and with HIRES on the Keck I 10 m telescope. The optical spectroscopy data demonstrate that RZ Psc is a pre-main sequence star with an effective temperature of  $5600 \pm 75$  K and  $\log g$  of  $4.35 \pm 0.10$ . The ratio of X-ray to bolometric luminosity,  $\log L_X/L_{\text{bol}}$ , lies in the range  $-3.7$  to  $-3.2$ , consistent with ratios typical of young, solar-mass stars, thereby providing strong support for the young-star status of RZ Psc. The Li absorption line strength of RZ Psc suggests an age in the range 30–50 Myr, which in turn implies RZ Psc lies at a distance of  $\sim 170$  pc. Adopting this estimated distance, we find the Galactic space velocity of RZ Psc to be similar to the space velocities of stars in young moving groups near the Sun. Optical spectral features indicative of activity and/or circumstellar material are present in our spectra over multiple epochs, which provide evidence for the presence of a significant mass of circumstellar gas associated with RZ Psc. We suggest that the destruction of one or more massive orbiting bodies has recently occurred within 1 au of the star, and we are viewing the aftermath of such an event along the plane of the orbiting debris.

## 1. Introduction

What is the nature of the enigmatic field star RZ Piscium (RZ Psc)? This curious case has been debated for decades (Potravnov et al. 2014b). There exists significant evidence that RZ Psc may be a young main sequence star with a dusty disk that is in the late stages of planet formation (de Wit et al. 2013; Grinin et al. 2015, and references therein). The star’s sharp dropouts in optical magnitude and its large IR excess have prompted the suggestion that a collisionally active asteroid belt is present in orbit around the star (de Wit et al. 2013; Kennedy et al. 2017). Such a scenario is similar to that proposed to explain UX Orionis objects, a class of young stars whose photometric variability is caused by variable circumstellar extinction (Herbst et al. 1994).

Indeed, most age estimates for RZ Psc are based on the assumption that RZ Psc is a UX Ori-type object. The age of RZ Psc was estimated from the equivalent width (EW) of the lithium 6708 Å line as  $\sim 10\text{-}70$  Myr, intermediate between the median ages of stars in the Pleiades and Orion clusters (Grinin et al. 2010). Potravnov & Grinin (2013) estimated an age of  $25 \pm 5$  Myr and concluded that the disk orbiting RZ Psc is in transition from primordial disk to debris disk.

However, it is worth considering whether RZ Psc might be an evolved star, given that aperiodic optical dropouts are also observed in such cases (e.g., WD 1145+017; Vanderburg et al. 2015). Indeed, RZ Psc’s high Galactic latitude ( $b \cong 35^\circ$ ) and lack of association with any known young stellar group might suggest evolved star status. If RZ Psc is an evolved giant, its disk may be a consequence of the destruction of a low-mass stellar companion or massive planet when the

star expanded to become a red giant. Melis (2009) chose to call such dusty, first ascent giant stars “Phoenix Giants” because of their similarities to T Tauri stars (specifically, high Li abundance and strong infrared excess; Potravnov et al. 2014b).

Furthermore, the strong IR excess associated with RZ Psc ( $L_{\text{IR}}/L_{\text{bol}} \sim 8\%$ , de Wit et al. 2013) would be very peculiar if the star is as old as  $\sim 25$  Myr. Typically, only cloud-embedded pre-main sequence stars have IR excesses this large (Figure 1 in Mamajek 2009). Many hundreds of young and main sequence solar-type stars have been studied over the past few decades (since the launch of the Infrared Astronomical Satellite), yet few have been found to have  $L_{\text{IR}}/L_{\text{bol}}$  as large as or larger than that of RZ Psc (examples are TYC 8241 2651 1 and V488 Per; Melis et al. 2012; Zuckerman et al. 2012). However, while RZ Psc’s level of IR excess is very unusual for a dusty debris disk, it is quite common for a Phoenix Giant (Zuckerman et al. 2008b; Melis et al. 2009; Melis 2009).

Attempts to distinguish between these evolutionary possibilities – i.e., a young star with a protoplanetary disk versus an evolved star with disk derived from the destruction of a companion – can be quite problematic. X-ray observations may provide key evidence about stellar properties that can break this degeneracy, as has been demonstrated in the case of BP Psc (Kastner et al. 2010). BP Psc was initially classified as a classical T Tauri star based on its strong  $\text{H}\alpha$  and forbidden line emission (Stephenson 1986), although it is located at high galactic latitude, far from any known star-forming regions. Zuckerman et al. (2008b) discovered an orbiting, dusty circumstellar disk and a parsec-scale system of highly collimated outflows, which is consistent with the classification of BP Psc as a pre-main sequence

star. However, the location of BP Psc in the sky, its weak lithium 6708 Å line, its gravity-sensitive photospheric absorption, the *Spitzer* Infrared Spectrograph spectrum of highly crystalline sub-micron-sized dust grains in its circumstellar disk (Melis et al. 2010), and the millimeter-wave molecular spectrum of its circumstellar disk are atypical for pre-main sequence (pre-MS) star-disk systems (Kastner et al. 2008). *Chandra* X-ray observations of BP Psc revealed that the star is a weak X-ray point source and its X-ray luminosity ratio ( $\log(L_X/L_{\text{bol}}) \sim -5.8$  to  $-4.2$ ) lies in the range that is observed for rapidly rotating (FK Com-type) G stars (Kastner et al. 2010). Hence, the *Chandra* results favor a scenario wherein the disk/jet system of BP Psc is the result of a very recent engulfment of a companion as the star ascended the giant branch.

To investigate whether the X-ray properties of RZ Psc might similarly discriminate between these potential competing models for its evolutionary state — i.e., young versus evolved star — we have obtained observations of the star with *XMM-Newton*. To further aid in determining the nature of the RZ Psc system, we obtained optical spectroscopic observations with the Hamilton Echelle on the Lick Shane 3 m telescope and with HIRES on the Keck I 10 m telescope. The observations and data reduction are described in Section 2, the results and analysis are described in Section 3, a discussion of the results is presented in Section 4, and a summary of the results and an outlook for future work is presented in Section 5.

## 2. Observations

### 2.1. *XMM-Newton* European Photon Imaging Cameras (EPIC)

RZ Psc was observed by *XMM-Newton* (Jansen et al. 2001) for  $\sim 38.8$  ks on 2015 January 2–3 during revolution 2759. The observations were conducted with the pn, MOS1, and MOS2 CCD arrays of the European Photon Imaging Cameras (EPIC) (Strüder et al. 2001; Turner et al. 2001) operating in full frame mode.

We also obtained simultaneous optical and UV observations with the Optical Monitor available on *XMM-Newton*. A summary of the *XMM-Newton* observations and exposure times is listed in Tables 1 and 2. Processing of the raw event data was performed, using standard methods, via the *XMM-Newton* Science Analysis System (SAS version 14.0).

In Figure 1, we present the merged EPIC pn, MOS1, and MOS2 X-ray images centered near the position of the target star. RZ Psc is the brightest of the few dozen X-ray sources detected in the observation. The associated X-ray source lies at  $01^{\text{h}}09^{\text{m}}42^{\text{s}}.05$ ,  $27^{\circ}57'01.95''$ , coincident with the near-IR position of RZ Psc (Figure 1, right).

### 2.2. High-Resolution Optical Spectroscopy

#### 2.2.1. *Lick Shane 3 m Hamilton Echelle*

RZ Psc was observed with the Shane 3 m telescope and Hamilton echelle spectrograph (Vogt 1987) at Lick Observatory. The observation dates and

parameters are listed in Table 3. Reduction of the Hamilton echelle data was performed using IRAF tasks following methods outlined in detail in Lick Technical Report No. 74<sup>1</sup>. Briefly, the spectral images were bias-subtracted, flat-fielded, extracted, and finally wavelength-calibrated with TiAr arclamp spectra (see Pakhomov & Zhao 2013).

### 2.2.2. Keck I 10 m HIRES

RZPsc was observed with the Keck I 10 m telescope at Maunakea Observatory, where echelle spectroscopy was performed with the HIRES instrument (Vogt et al. 1994). Observation dates and parameters are listed in Table 3. All of the HIRES data were reduced with the MAKEE software package. The spectral images were bias-subtracted and flat-fielded, then the spectra were extracted and finally wavelength-calibrated with ThAr arclamp spectra.

## 2.3. Keck II 10 m Echellette Spectrograph and Imager (ESI)

A candidate M-type companion to RZPsc (see§ 3.7) was observed at Maunakea Observatory with the Keck II 10 m telescope. Echelle spectroscopy was performed with the ESI (Sheinis et al. 2002), and observation parameters are given in Table 3.

Data were reduced with standard IRAF tasks and procedures similar to the reduction of Hamilton data as described above. Specifically, spectral images were

---

<sup>1</sup>See <http://astronomy.nmsu.edu/cwc/Software/irafman/manual.html>.

bias-subtracted, flat-fielded with the use of dome flat exposures, extracted, and wavelength-calibrated with the use of CuArXeHgNe arc lamps.

#### 2.4. WIYN-0.9 m Half Degree Imager (HDI)

RZPsc and its field were observed at Kitt Peak National Observatory with the WIYN 0.9 m telescope<sup>2</sup> in 2016 January. The HDI was used to take 10 s exposures of the RZPsc field in BVRI filters.

Data were reduced with standard AstroImageJ tasks and procedures (Collins et al. 2017). Multi-aperture differential photometry was then performed to determine the magnitude of stars in the field in all bands.

### 3. Results and Analysis

In Table 4, we present the key characteristics of RZPsc that we have gleaned from the literature, and in Table 5, we present the key characteristics determined via the analysis described next.

---

<sup>2</sup>The WIYN Observatory is a joint facility of the University of Wisconsin-Madison, Indiana University, the National Optical Astronomy Observatory and the University of Missouri.



### 3.1. Model Atmosphere Analysis

An LTE, 1D model atmosphere analysis of the optical spectra of RZ Psc obtained with the Keck and Shane telescopes was performed using the spectrum synthesis program Moog (Snedden 1973, 2014 version) to determine the atmospheric parameters and composition of the star. Model atmospheres have been interpolated within the MARCS4 grid (Gustafsson et al. 2008). The line list of Yong et al. (2014) was adopted for atomic data.

Equivalent widths (EWs) were first measured for individual spectra using the *plot* task in IRAF<sup>3</sup>. Measurements from different epochs were compared to identify any systematic differences in line strength at different epochs. Since no variations in EWs were found, seven spectra covering a range of dates from 2013 through 2016 were co-added to produce a spectrum of higher S/N ratio; the combined spectrum has a S/N ratio of 200. The combined spectrum with lower noise also reduces the uncertainty in the continuum level, allowing more accurate determination of EWs. The final EWs used for the analysis were measured from the combined spectra.

The first step was to carry out the determination of atmospheric parameters – effective temperature, surface gravity, microturbulence, and metallicity – independently of previous determinations. We selected 101 lines of Fe I to cover a range of both line strength and excitation potential, and model atmosphere

---

<sup>3</sup>IRAF is distributed by the National Optical Astronomy Observatory, which is operated by the Association of Universities for Research in Astronomy (AURA) under a cooperative agreement with the National Science Foundation.

parameters were varied to minimize the dependence of derived abundance on EW and excitation potential. The procedure yielded an effective temperature of  $5600 \pm 75$  K and a microturbulence of  $v_T = (2.0 \pm 0.2)$  km s<sup>-1</sup>. The surface gravity of the star was determined to be  $\log g = 4.35 \pm 0.10$  by minimizing the difference in the Fe abundance derived from Fe I and Fe II lines. The resulting metallicity is  $[\text{Fe}/\text{H}] = -0.11 \pm 0.03$  (standard error of the mean or S.E.M.), not including systematic errors in the atmospheric parameters.

Abundances of additional species were determined once the model atmosphere parameters were established. Again, the Yong et al. (2014) line list provided atomic data. The derived abundances are included in Table 6, along with estimated uncertainties, including both random and systematic errors, where the solar abundances are taken from Asplund et al. (2009). The uncertainties in the atmospheric parameters are determined from the parameter change needed to establish a clear dependence of abundance versus excitation potential or abundance versus line strength, or a difference in abundance as derived from Fe I and Fe II lines.

Atmospheric parameters for RZ Psc have previously been reported by Kaminskiĭ et al. (2000) and by Potravnov et al. (2014b). Kaminskiĭ et al. reported a weighted average temperature of 5250 K based on their analysis of three spectra with S/N ratios in the range 44-68 and a spectral resolving power of  $R \approx 25,000$ . They employed three alternate methods, including an unreddened color-temperature relation, specific line ratios, and, as we used here, a minimization of the dependence of abundance on excitation potential for Fe I lines, the “Boltzman equilibrium.” For

this last method, they derived an effective temperature of  $5450 \text{ K} \pm 150 \text{ K}$ , which is statistically indistinguishable from our best fit temperature of  $5600 \pm 75 \text{ K}$ . Although their result for microturbulence ( $v_T = 2.0 \pm 0.5 \text{ km s}^{-1}$ ) agrees with ours, their determination of  $\log g = 3.41 \pm 0.02$  is discrepant.

Potravnov et al. (2014b) analyzed a higher-resolution spectrum ( $R \approx 46,000$ ) with a S/N ratio of about 75. Their temperature of  $5350 \text{ K} \pm 150 \text{ K}$  was obtained from synthetic spectrum fits to a few features, most notably  $\text{H}\alpha$  and  $\text{H}\beta$ , which may be compromised by circumstellar emission. With the temperature fixed at 5350 K, they used SME analysis software (Valenti & Piskunov 1996) to determine  $\log g = 4.2 \pm 0.3$  and  $v_T = 1 \text{ km/s}$ .

To attempt to resolve the discrepancies among these model fits, we determined the elemental abundances of RZ Psc using each of the three Kaminskiĭ et al. (2000) models with our measured EWs. The Kaminskiĭ et al. atmospheric parameters provide a consistent abundance for the Fe I and Fe II lines but significant deficiencies in the abundances of the ionized species Sc II and Ti II. We note that the abundances listed in their Table 3 include large deficiencies of Ti, V, Cr, and Ni, as well as Si and Al.

The Potravnov et al. model atmosphere parameters with our EWs suggest that a value of  $2 \text{ km s}^{-1}$  for the microturbulence provides a better fit. With that correction, adopting the Potravnov et al. model leads to a significant discrepancy ( $\Delta[\text{Fe}/\text{H}] = 0.2 \text{ dex}$ ) between the Fe I and Fe II lines, as well as a low abundance of Fe compared to other metals.

Our adopted model parameters provide both a good match for the Fe I and

Fe II lines and a reduced dispersion in the abundances of other species compared to either the Kaminskiĭ et al. or the Potravnov et al. models, and we conclude that our adopted model atmosphere parameters provide the best description of the atmosphere of RZ Psc at the epochs of our observations. Our model yields an overall iron abundance  $[\text{Fe}/\text{H}] = -0.1$  for RZ Psc.

Using the adopted model and the average Li EW of 207 mÅ we obtain a lithium abundance of  $A(\text{Li}) = 3.05^4$  for RZ Psc. This analysis uses the Li I line list from Reddy et al. (2002), including a six-component blend of the various explicit features that make up the  ${}^7\text{Li} + {}^6\text{Li}$  feature, and assumes a standard isotopic ratio of 10/1.

### 3.2. Spectral Type

Spectral types ranging from early K to late G have been assigned to RZ Psc in the literature thus far (e.g., Herbig 1960; Kaminskiĭ et al. 2000). It appears that RZ Psc is not a main sequence star, given optical spectral diagnostics that are indicative of low surface gravity (Kaminskiĭ et al. 2000, § 3.1). Our determination of an effective temperature of 5600 K and surface gravity of  $\log g = 4.35 \pm 0.10$  is consistent with a luminosity class of type III/IV. The latter implies that RZ Psc must be either a pre-main sequence star or an evolved star (giant). Adopting this temperature and the empirical spectral type-temperature sequence for 5-30 Myr old

---

<sup>4</sup> $A(x) = 12 + \log n(x)/n(\text{H})$ , where  $n(x)$  is the number density of atoms of species  $x$  and  $n(\text{H})$  is the number density of H atoms.

pre-main sequence stars presented in Pecaut & Mamajek (2013), RZ Psc appears to have a spectral type of G4 if it is in a pre-main sequence evolutionary stage, but as Herbig (1960) originally noted, the photospheric features of RZ Psc correspond to a later spectral type, K0 IV.

### 3.3. Stellar Activity and Rotation

We examined Lick/Hamilton and Keck/HIRES optical spectra for RZ Psc for indications of stellar activity. Typical features indicative of activity include  $H\alpha$  emission and core-reversal emission in the Ca II H, K, and infrared triplet lines. Figure 2 showcases the dramatic variability displayed by RZ Psc in the  $H\alpha$  region. Variability in the strength of the photospheric absorption component of  $H\alpha$  is evident, as is an additional, presumably circumstellar component that sometimes appears as broad absorption wings around the  $H\alpha$  absorption line core (e.g., 2013 August 14, 2013 October 16, and 2013 November 14; see also Kaminskiĭ et al. 2000) or, perhaps, as a stronger core absorption component (2013 November 16; all three spectra for the 2013 November 16 epoch have the same appearance to within their relative S/N). Emission above the continuum level also appears at multiple epochs.

The highly variable  $H\alpha$  line profile of RZ Psc, including the appearance of emission above the stellar continuum, is reminiscent of those of certain young stars that are rotating at near-breakup speeds and are possibly losing mass (e.g., Marcy et al. 1985; Stauffer et al. 1989). However, the  $v \sin i$  of RZ Psc (at most 23 km/s, see Table 4) is well below breakup speeds and is otherwise consistent with those of young cluster stars that display similar levels of X-ray activity

(e.g., Stauffer et al. 1997, their Figure 6). This suggests a different origin for the circumstellar gas that is responsible for the variable H $\alpha$  emission from RZ Psc; we explore one potential explanation in Section 4.4.

For each H $\alpha$  emission epoch we calculated the full-width of the double-peaked structures at 10% of the peak line flux. We find that the emission structures have velocity widths  $\gtrsim 300 \text{ km s}^{-1}$ . Thus, as was concluded by Stauffer et al. (1989) and Marcy et al. (1985) for their rapidly-rotating stars, the H $\alpha$ -emitting material is unlikely to be located at the stellar surface and instead is either being ejected in a wind or is orbiting or infalling within a few stellar radii of RZ Psc.

Steadier emission likely associated with stellar activity is seen in the Ca II H and K lines (Figure 3). In some epochs, a blueshifted absorption component is seen adjacent to the emission line, while the UT 2013 November 13 epoch shows a much broader emission line than is seen in other epochs. It should be noted that the spectrum of UT 2013 November 13 is particularly noisy, perhaps as a result of RZ Psc being observed during during one of its deep optical minima. The enhanced H $\alpha$  emission observed during this observation would be consistent with the star being heavily obscured by dust; such behavior is observed, e.g., in the case of the highly inclined for T Cha star/disk system (Schisano et al. 2009). Ca II infrared triplet core-reversal emission is evident in the UT 2013 21 October 21 epoch and some emission is present in the UT 2013 November 16 epoch (Figure 4), although its nature is not immediately obvious given the complex structure in the lines. The high velocity of the emitting material intermittently seen in H $\alpha$  provides evidence for a wind from (or infall onto) the surface of the star. A similar behavior was

observed by Potravnov et al. (2017).

Figure 5 displays the spectral region around the Na I D lines. Clear variability is evident, with blueshifted absorption features regularly appearing and moving away from the photospheric absorption components. Such behavior was noted by Grinin et al. (2015), and served as the basis for their hypothesis that RZ Psc is in the so-called “propeller” regime of mass loss due to a combination of strong magnetic field and low accretion rate.

### 3.4. Radial Velocities

In order to derive RZ Psc’s radial velocity (RV) at each epoch, we cross-correlated each of the HIRES and Hamilton spectra with spectra of stars with known radial velocities from Nidever et al. (2002). This process also allowed us to search for any radial velocity variability between epochs. Each of the HIRES and Hamilton spectra yields radial velocity measurements for RZ Psc with precision of roughly  $0.2 \text{ km s}^{-1}$  (Table 7). Excluding the UT 2013 November 13 epoch, there appears to be significantly detected radial velocity variability at the few  $\text{km s}^{-1}$  level. This variability appears to be centered on a systemic velocity of roughly  $-1 \text{ km s}^{-1}$ , consistent with the radial velocity measurement determined by Potravnov et al. 2014a, and does not have any obvious periodicity. Such measurements seem at odds with the radial velocity of  $-11.75 \pm 1.1 \text{ km s}^{-1}$  measured by Kaminskiĭ et al. (2000).

The velocity we determine from the Hamilton spectrum obtained on UT

2013 November 13 appears as a notable outlier when compared to almost all previous radial velocities measured for RZ Psc, apart from the Kaminskiĭ et al. (2000) measurement. At this epoch (UT 2013 November 13) the cross-correlation peak splits into two components (Figure 6; i.e., a redshifted absorption line and a weaker blueshifted component). Indeed, when the UT 2013 November 13 spectrum is smoothed, a similar morphology is evident in some absorption lines that is not present in the UT 2013 November 14 spectrum. A deblending fit to the cross-correlation double-peak was performed using the FXCOR task within IRAF, and the resulting velocities for each peak (corrected to the heliocentric reference frame) are reported in Table 7. The unusually large negative velocity of the blue peak of the cross-correlation function for 2013 November 13 is marginally consistent with the velocity for RZ Psc determined by Kaminskiĭ et al. (2000)<sup>5</sup>.

### 3.5. Modeling the X-ray Spectrum of RZ Psc

Source X-ray spectra were extracted from the *XMM* pn, MOS1, and MOS2 event lists by selecting photon events within circular regions with diameters of  $\sim 25\text{-}40''$  centered on RZ Psc (Figure 1). Associated background spectra were extracted within circular regions with the same diameters from nearby, source-free regions. We fit the resulting background-subtracted spectra of RZ Psc with the

---

<sup>5</sup>Unfortunately, it is not clear at which of these epochs (1991 December or 1998 August) Kaminskiĭ et al. (2000) obtained this discrepant radial velocity measurement.



HEASOFT *Xanadu*<sup>6</sup> software package (version 6.16), using XSPEC<sup>7</sup> version 12.8.2. The pn, MOS1, and MOS2 X-ray spectra of RZ Psc, displayed in Figure 7, were analyzed using three different models over the range 0.15-10 keV. Each of the adopted models (see below) made use of the XSPEC optically thin thermal plasma model *vapec* (Foster et al. 2012)<sup>8</sup>, which is parameterized by plasma elemental abundances, temperature, and emission measure (indirectly, through the model normalization). We included the potential effects of intervening absorption by using XSPEC’s *wabs* absorption model (Morrison & McCammon 1983). All of our models include two temperature components, as required by the  $\chi^2$  statistics. The fixed and free parameters for all three models are displayed in Table 8, with the free parameters having associated uncertainty values.

Since the evolutionary status of RZ Psc was unclear to us, we adopted models that were representative of young stars and evolved stars. The first model, hereafter referred to as “T Tauri Star,” uses plasma abundance parameter values that represent average values for T Tauri stars in Taurus (Skinner & Güdel 2013, and references therein); these values are stated in Table 8. For the second model, hereafter referred to as “Evolved Giant Star,” we fixed the parameters for the plasma abundances to values that have been determined to be typical for chromospherically active late-type giants (Gondoin 2003a,b,c). In the third model, designated “Free Abundance,” we allowed the abundances of Ne, Fe, and C to be

---

<sup>6</sup>See <http://heasarc.gsfc.nasa.gov/docs/xanadu/xanadu.html>.

<sup>7</sup>See <http://heasarc.gsfc.nasa.gov/xanadu/xspec>.

<sup>8</sup>See <http://www.atomdb.org>.

free parameters. Lines of the first two elements likely dominate the emission around the spectrum peak ( $\sim 0.3\text{-}3$  keV) in the relevant ( $\sim 10$  MK) temperature regime (see, e.g., Kastner et al. 2002). We allowed the abundance of C to be a free parameter in order to fit the spectral feature near 0.3-0.4 keV.

The results of the spectral analysis are presented in Table 9 and Figure 7. Adopting  $D = 174$  pc (see § 4.1), we find a range of X-ray luminosities,  $L_X$ , from  $\sim 5.9 \times 10^{29}$  to  $\sim 1.5 \times 10^{30}$  ergs s $^{-1}$ , depending on the model adopted. The T Tauri and Evolved Giant models yield best-fit values of  $L_X$  that are very similar and lie at the lower end of this range. The corresponding range of best fit  $N_H$  values are as small as  $\sim 4 \times 10^{20}$  cm $^2$  and as large as  $\sim 2 \times 10^{21}$  cm $^2$ . The fit results for all three models indicate that the emission measures are similar for both temperature components, with the low- and high-temperature components lying in the ranges  $\sim 3 - 9$  MK and  $\sim 10 - 20$  MK, respectively.

### 3.6. *XMM-Newton* Optical Monitor Data

The *XMM* Optical Monitor (OM) photometry was used to determine UBVM and UVM2 magnitudes of RZ Psc simultaneously with the X-ray measurements. These OM measurements thereby allow us to determine the star’s bolometric flux  $F_{\text{bol}}$  during the X-ray observations, alleviating uncertainties in determining  $L_X/L_{\text{bol}}$  that could arise due to the significant optical variability and likely X-ray variability of RZ Psc. The OM photometry is provided in Table 2. It is evident that the star’s flux remained constant in all four passbands during the observations. Based on V-band magnitude obtained with the OM we further conclude that, during our

*XMM* observations, RZ Psc was not undergoing one of its rare, deep visual minima, which can be as dim as  $V \sim 14$  (de Wit et al. 2013). Adopting the mean  $V$ -band magnitude obtained from the OM photometry and assuming bolometric corrections based on the adopted effective temperature and luminosity class of RZ Psc (see Section 3.2), we obtain  $F_{\text{bol}}$  values that range from  $\sim 6.7 \times 10^{-10}$  to  $\sim 6.9 \times 10^{-10}$  erg s $^{-1}$  cm $^{-2}$ . Adopting a distance of 170 pc to RZ Psc (see § 4.1), we obtain a bolometric luminosity  $L_{\text{bol}} \sim 0.6 L_{\odot}$  (excluding any contribution from circumstellar dust).

From the OM photometric results and the adopted effective temperature, which implies  $(B - V)_0 = 0.66$ , we estimate the optical extinction of this system at the time of our *XMM-Newton* observations to be  $A_V \sim 0.66$  (assuming  $R = 3.09$ ; Rieke & Lebofsky 1985). Our estimated value of  $A_V$  is larger than the value of  $0.3 \pm 0.05$  quoted in Potravnov et al. (2017). The discrepancy between these values of  $A_V$  are consistent with the optical dropout behavior associated with RZ Psc.

### 3.7. Search for Comoving Low-Mass Stellar Companions

The high galactic latitude of RZ Psc (see Table 4) and its large displacement from any known nearby young moving group (see Table 1 of Mamajek 2016) are problematic for a young star scenario. Thus, we used the pipeline-generated X-ray source list compiled from the *XMM-Newton* observation as the basis for a search for young, X-ray active stars that are comoving with RZ Psc.

The *XMM-Newton* images were matched to images from the WIYN 0.9m

telescope and the 2MASS and *WISE* image archives to identify optical and IR sources coincident with (i.e., within 2 of) those XMM X-ray sources lying within approximately 15' of RZ Psc. This yielded seven X-ray sources with optical/IR counterparts, which we regarded as candidate comoving stars. Spectral Energy Distributions (SEDs) for these seven sources were produced using magnitudes obtained from the WIYN 0.9m images, along with those available in the 2MASS and *WISE* catalogs. The resulting SEDs were then fit with stellar atmosphere models<sup>9</sup> (Castelli & Kurucz 2003). This SED analysis and comparison of the proper motions of these seven candidates with that of RZ Psc eliminated all but one of these objects as possible members of a nearby moving group associated with RZ Psc. This object, J0109+2758, is an M-type star at a separation of 2.3' from RZ Psc (Gingerich et al. 2017). J0109+2578 was only detected by *XMM*, and hence considered as a candidate comoving star, due to a strong flare during the exposure. Gingerich et al. (2017) concluded that J0109+2578 was a main sequence M flare star which, if associated with RZ Psc, would provide evidence in favor of an evolved star status.

To confirm the spectral type and evolutionary status of J0109+2578, we obtained a spectrum with the ESI on Keck II. Comparison with spectral templates in Jacoby et al. (1984) confirms that J0109+2578 is an M dwarf. The Keck/ESI spectrum of J0109+2758 was cross-correlated with a spectrum of NLTT 853 (Nidever et al. 2002) that was obtained on the same night as J0109+2758 with the

---

<sup>9</sup>The stellar atmosphere models were obtained from the Castelli and Kurucz grids of model atmospheres: <http://kurucz.harvard.edu/grids.html>.

same setup. From the cross-correlation, we measure a heliocentric radial velocity for J0109+2758 of  $-33.5 \pm 1.5 \text{ km s}^{-1}$ , clearly discrepant with the approximate median radial velocity of RZ Psc ( $V_r \sim -2 \text{ km s}^{-1}$ , see Table 7). Thus, we conclude that J0109+2758 is not comoving with RZ Psc and hence is not associated with it.

## 4. Discussion

### 4.1. Age Diagnostics: Stellar Activity and Li Line Strength

Our *XMM-Newton* observations reveal that RZ Psc is highly X-ray active, with  $\log(L_X/L_{\text{bol}})$  in the range  $-3.7$  to  $-3.2$  (§ 3.5). This large fractional X-ray luminosity is consistent with the enhanced presence of activity indicators in the optical spectrum of RZ Psc (§ 3.3). Such levels of X-ray activity are primarily associated with late-type, short-period binaries (e.g., RS CVn systems) or rapidly rotating, late-type single stars (Berdyugina 2005; Gondoin 2005, and references therein). Stars in the latter category are generally either young — i.e., in the T Tauri, post-T Tauri, or zero-age main sequence stages — or are particularly fast-rotating evolved giants (e.g., stars of the FK Com class). However, whereas virtually all young stars with effective temperatures similar to RZ Psc (i.e., G type stars) have values of  $L_X/L_{\text{bol}}$  in the range we determine for RZ Psc (e.g., Randich et al. 1995, see their Figure 6), very few rapidly rotating giants have such large relative X-ray luminosities (Gondoin 2005). Thus, in contrast to the case of BP Psc (Kastner et al. 2010), the value of  $\log(L_X/L_{\text{bol}})$  obtained from our X-ray observations strongly favors young-star status for RZ Psc.

Our measurement of a large value of  $\log(L_X/L_{\text{bol}})$ , which is indicative of strong surface magnetic activity, supports the hypothesis that RZ Psc is in the “magnetic propeller” regime of efficient mass loss relative to its accretion rate (Grinin et al. 2015). To attempt to better determine the nature of the X-ray emission from RZ Psc, it would be beneficial to obtain high-resolution (gratings) X-ray spectra of the star, from which we can obtain the detailed emission-line spectrum of the X-ray emitting plasma. Such data might establish, e.g., whether the composition of this plasma resembles those characteristic of the X-ray-emitting plasma of pre-main sequence stars and whether some of the X-ray emission from RZ Psc may arise from accretion activity (e.g., Brickhouse et al. 2010).

Our measurement of the EW of the Li I line, averaged over all epochs, is  $207 \pm 6 \text{ m}\text{\AA}$ , consistent with that measured by Grinin et al. (2010). This EW(Li) measurement is somewhat less than those of 10-20 Myr old G-type stars (see Figure 6, Spina et al. 2014), but is consistent with G-type stars of ages 30-50 Myr (Table 2, Randich et al. 2001 and Figure 3, Zuckerman & Song 2004). The EW(Li) of RZ Psc is somewhat larger than that of G-type stars in the Pleiades (Soderblom et al. 1993), but consistent with such stars in the  $\beta$  Pictoris Moving Group (age  $\sim 23 \pm 3$  Myr; Mamajek 2016) and the Tucana-Horologium Association (age  $\sim 45 \pm 5$  Myr; Mamajek 2016) (see Figure 5; Mentuch et al. 2008).

Comparing with Table 1 in Soderblom et al. (1993), we estimate  $A(\text{Li}) \sim 3.0$  for RZ Psc, consistent with the value of 3.05 that we calculated in sec 3.1. Although there are approximately 40 examples of Li-rich giants with such large lithium abundances (e.g., Casey et al. 2016), almost all of these giants have much smaller

values of  $\log g$  ( $\log g < 3$ ) than RZ Psc ( $\log g \sim 4.35 \pm 0.1$ ).

In light of this evidence for pre-main sequence status, we have conducted an H-R diagram analysis with theoretical pre-main sequence isochrones to estimate the likely range of luminosity of RZ Psc. Following our Li EW analysis, we assume an age range of 30-50 Myr for RZ Psc. The resulting H-R diagram is displayed in Figure 8, where the isochrones and pre-main sequence tracks overlaid are obtained from PARSEC<sup>10</sup> (the PAdova and TRieste Stellar Evolution Code; Bressan et al. 2012). Figure 8 suggests that RZ Psc is a pre-main sequence star of mass 0.75-1.0  $M_{\odot}$ . Our H-R diagram analysis yields  $\log(L_*/L_{\text{bol}})$  in the range of  $-0.08$  to  $-0.21$ , which corresponds to a distance to RZ Psc of  $\sim 186$  pc if RZ Psc is 30 Myr old and a distance of  $\sim 161$  pc if RZ Psc is 50 Myr old. This estimated distance range, obtained from our Li- and X-ray-based age range, agrees with the distance estimate of 160 pc mentioned in Potravnov et al. (2017, and references therein). Our age and mass estimates are also similar to the values cited by those authors ( $25 \pm 5$  Myr and  $1 M_{\odot}$ , respectively).

Finally, we consider the  $UVW$  velocities of RZ Psc. Adopting a median estimated distance of 170 pc, the Table 4 proper motion, and a median radial velocity of  $-2 \text{ km s}^{-1}$  (Table 7), the  $UVW$  are  $-13.4, -18.2, -5.4 \text{ km s}^{-1}$ .<sup>11</sup> These  $UVW$  values are consistent with young star status – the closest kinematic matches being to the TW Hya Association,  $\beta$  Pic moving group, and the Columba Association (Mamajek 2016). However, RZ Psc is much further from Earth than

---

<sup>10</sup><http://stev.oapd.inaf.it/cgi-bin/cmd>

<sup>11</sup><http://kinematics.bdnyc.org/query>

established members of these groups.

#### 4.2. X-ray Absorption versus Optical Extinction

In Figure 9, we compare the range of the gas column density we determine from the photoelectric absorption of the X-rays emitted by RZ Psc,  $N_H \sim (0.4-1.8) \times 10^{21} \text{ cm}^{-2}$  (§ 3.5) with the estimate of visual extinction due to dust ( $A_V$ ) along the line of sight to the star afforded by the simultaneous *XMM-Newton* OM data (§ 3.6).

These measurements for RZ Psc are overlaid over empirical  $N_H$  versus  $A_V$  curves for the local ISM and the  $\rho$  Ophiuchi molecular cloud. The figure demonstrates that the relation between absorption and extinction toward RZ Psc is consistent with that of the ISM if we adopt the “Free Abundance” model; i.e., the model results in an  $N_H$  that is most consistent with an  $A_V$  given ISM-like grains. Adopting either of the other X-ray spectral models would imply that the gas-to-dust ratio of the circumstellar material may differ significantly from that of the ISM or  $\rho$  Oph. Such an interpretation of Figure 9 is subject to the important caveat that, because the OM  $V$  photometry indicates that RZ Psc was observed in a relatively low-extinction state, we cannot ascertain whether the observed relationship between  $N_H$  and  $A_V$  toward RZ Psc at the time of our observations was representative of the intervening ISM or of circumstellar material associated with RZ Psc itself.



### 4.3. The Puzzling Radial Velocity Behavior of RZ Psc

In our radial velocity (RV) cross-correlation analysis, we find marginal evidence for RV variability, including one epoch in which the cross-correlation function appears double-peaked (Figure 6). One possibility that could account for this potential RV variability is that RZ Psc may reside in a spectroscopic binary system, one that can, on rare occasions, be double lined. This would make RZ Psc superficially similar to BD+20 307, which also has a large value of  $L_{\text{IR}}/L_{\text{bol}}$ , thought to be the result of a catastrophic collision of terrestrial mass planets (Zuckerman et al. 2008a).

If RZ Psc is indeed a spectroscopic binary, then there would be a new, interesting route through which we could explore the age and evolutionary status of the system. If both stars are pre-main sequence, then both should have comparably strong lithium absorption. We examined the line shape of the UT 2013 November 13 Li I  $\lambda 6708$  line to see if it shows a blueshifted shoulder. First, the EW of the Li I line was measured in all epochs. To within the uncertainties of each epoch, these EWs agreed. Next, a smoothed Li I line was compared to other comparably strong lines at similar wavelengths, most notably the Ca I  $\lambda 6717$  line. While the Ca I line showed an obvious slightly weaker blueshifted shoulder, the Li I line did not. Finally, cross-correlations were performed between the UT 2013 November 13 spectrum of RZ Psc and other stars using only single lines. Most single lines showed either double-peaked cross-correlation maximums or significant broadening in the blueshifted region where the second peak would be expected. The Li I line, in contrast, was well fit with a single gaussian and showed no signs of blueshifted

broadening. The velocity of the Li I line, however, does not match either velocity measured on UT 2013 November 13 via cross-correlation analysis, but rather lies in between that of these two velocity signals. This complication makes it difficult to interpret the Li I as present in only one star in a putative binary system.

#### **4.4. What is the Origin of the Circumstellar Material Orbiting RZ Psc?**

The extreme dropout events in the optical light curve of RZ Psc invite comparisons between this system and objects showing similarly dramatic dropouts, such as the variable field star KIC 8462852 (aka “Tabby’s Star”; Boyajian et al. 2016) and the remarkable “polluted” white dwarf WD 1145+017 (e.g., Rappaport et al. 2016). The profound, seemingly aperiodic, variability observed in both of those cases has been cited as evidence for the presence of orbiting and/or infalling circumstellar debris arising either from a catastrophic collision or tidal stripping of a subplanetary-mass body or bodies. Xu et al. (2016) suggest that the atomic absorption lines observed in the spectrum of WD 1145+017 could come from either a burst of accretion due to disintegrating planetesimals, a previous tidal disruption, or both.

As in the case of WD 1145+017, which displays wide and variable gaseous absorption lines in its spectrum that are indicative of a gas-rich disk (Xu et al. 2016), the presence of rapidly variable emission and absorption in the wings of RZ Psc’s  $H\alpha$  line profiles (Figure 2) suggests that its orbiting debris includes a significant gaseous component. However, in terms of evolutionary state and, hence, the nature of the disrupted orbiting body or bodies, the (G-type) RZ Psc

system would appear to have more in common with (F-type) KIC 8462852 than WD 1145+017. Indeed, a major difference between the RZ Psc and KIC 8462852 systems would appear to be that the circumstellar mass associated with RZ Psc is far larger than that associated with KIC 8462852. Specifically, unlike RZ Psc, KIC 8462852 does not have a detectable IR excess, and its optical dropouts are far less pronounced; whereas RZ Psc suddenly dims by several magnitudes (de Wit et al. 2013), the sudden dips in flux exhibited by KIC 8462852 are of the order of  $\sim 20$  percent or less (Boyajian et al. 2016). This suggests that the putative body (or bodies) destroyed around RZ Psc was far more massive than in the case of the KIC 8462852 system, whose debris has variously been attributed to a rocky body originally a few hundred km in diameter with a mass of at most  $10^{-6}$  Earth masses (Boyajian et al. 2016) or to a handful of disintegrating cometary bodies (Neslušan & Budaj 2017).

We hence propose that the puzzling variability behavior and enormous infrared excess of RZ Psc is most readily ascribed to the aftermath of the recent tidal disruption of a substellar companion or giant planet, or a catastrophic collision involving one or more relatively massive, gas-rich orbiting bodies. Evidently, as in the cases of KIC 8462852 and WD 1145+017, the enormous dips in the optical light curve of RZ Psc require that the orbiting debris resulting from this destructive event is confined to a disk that lies nearly along our line of sight to the star. Although the bulk of the dusty debris is likely orbiting  $\sim 0.3$  au from the star (based on the temperature of the dust excess,  $\sim 500$  K; de Wit et al. 2013), the broad absorption features in the  $H\alpha$  line profiles of RZ Psc indicate that at least some of the circumstellar material is either accreting onto the star, outflowing, or both.

Although the preponderance of evidence appears to support the young star status of RZ Psc, there are some caveats to be considered. The consumption of a giant planet or substellar companion could be polluting the atmosphere of RZ Psc, thereby increasing the atmospheric abundance of Li, which would make the star appear younger than it is (see, e.g., Sandquist et al. 2002). Our measured (relatively low) value of  $\log g$  could similarly be explained by accretion of debris from a substellar-mass companion, given that the primary would be expected to expand during the accretion process. Indeed, it is possible that  $\log g$  may be variable as a consequence of this (presumably ongoing) planet or substellar companion consumption process. Accretion of material from a disrupted massive body would also increase the magnetic activity of the star, and hence might also explain the prodigious X-ray output of RZ Psc. Thus, we should look to *Gaia*'s forthcoming determination of the parallax distance and refinement of the space velocity of RZ Psc as the prime means to verify its youth.

## 5. Summary and Conclusions

We have used *XMM-Newton*, along with high-resolution optical spectroscopy, to characterize the properties of the infrared-excess, variable star RZ Psc so as to confirm its evolutionary status. The *XMM-Newton* observations produced a detection of a bright X-ray point source coincident with the centroids of optical and infrared emission at RZ Psc, with the log of the ratio of X-ray to bolometric luminosity,  $\log L_X/L_{\text{bol}}$ , in the range  $-3.7$  to  $-3.2$ . These results are consistent with  $\log L_X/L_{\text{bol}}$  ratios typical of low-mass, pre-main sequence stars, and larger than

that of all but the most X-ray-active stars among giants (e.g., FK Com-type giants). Examination of the X-ray sources in the RZ Psc field yields one candidate comoving (M dwarf) star, but the radial velocity of this potential wide (2.3' separation) companion is inconsistent with that of RZ Psc.

High-resolution optical spectra obtained with the Hamilton Echelle on the Lick Shane 3 m telescope and HIRES on the Keck I 10 m telescope indicate that RZ Psc has an effective temperature and a surface gravity that are consistent with a pre-main sequence star. Sporadic radial velocity variability may also be observed in RZ Psc; if confirmed, this would suggest that it may be a spectroscopic binary system. We note that the potential radial velocity variability and bizarre  $H\alpha$  emission-line profile variability observed for RZ Psc are both reminiscent of the 5-10 Myr old star T Cha, which also exhibits deep absorption episodes, like RZ Psc, due to an inclined dusty disk (Schisano et al. 2009).

The *XMM-Newton* and high-resolution optical spectroscopy results favor a young star status for RZ Psc. Measurements of the Li EW indicate that RZ Psc is a  $\sim 30$ -50 Myr old post-T Tauri star. If the age of RZ Psc is indeed this advanced, the presence of significant, varying column densities of circumstellar gas and dust renders it extremely unusual among Sun-like pre-main sequence stars. By analogy with objects such as KIC 8462852 (aka “Tabby’s Star”; Boyajian et al. 2016) and WD 1145+017 (e.g., Rappaport et al. 2016), it is possible that, in the RZ Psc system, we are seeing evidence of a catastrophic event, for example, the destruction of a massive planet. Optical spectral features indicative of activity and/or circumstellar material, such as core-reversal emission in the Ca II H, K,

and infrared triplet lines and  $H\alpha$  emission, are present in our spectra over multiple epochs, and provide evidence for the presence of a significant mass of circumstellar gas associated with RZ Psc. The presence of a significant mass of circumstellar gas (as reflected in the broad  $H\alpha$  emission-line profiles) might imply that the cannibalized planet was a hot Jupiter.

An H-R diagram analysis indicates a distance to RZ Psc of  $\sim 170$  pc if RZ Psc is a pre-main sequence star. *Gaia* should provide the parallax distance and space velocity measurements necessary to nail down the evolutionary status of RZ Psc and to refine estimates of its age. Further observations are warranted to understand the nature of this enigmatic star: high-resolution X-ray spectroscopy of RZ Psc would improve constraints on the abundances of RZ Psc’s X-ray-emitting plasma; an optical and infrared spectroscopy campaign would shed light on the potential binary nature of the system; and submillimeter interferometric imaging and optical/IR coronagraphic adaptive optics imaging would establish whether there is cold, extended gas and dust associated with the RZ Psc disk.

*This research was supported in part by NASA Astrophysics Data Analysis program grant NNX16AG13G to RIT. Carl Melis acknowledges NASA Astrophysics Data Analysis program grant ADAP13-0178. This paper is based in part on observations at Kitt Peak National Observatory, National Optical Astronomy Observatory (NOAO), which is operated by the Association of Universities for Research in Astronomy (AURA) under a cooperative agreement with the National Science Foundation. Some of the data presented herein were obtained at the W. M. Keck Observatory, which is operated as a scientific partnership among the California*

*Institute of Technology, the University of California and the National Aeronautics and Space Administration. The Observatory was made possible by the generous financial support of the W. M. Keck Foundation. The authors wish to recognize and acknowledge the very significant cultural role and reverence that the summit of Maunakea has always had within the indigenous Hawaiian community. We are most fortunate to have the opportunity to conduct observations from this mountain. We thank the referee Ilya Potravnov for an insightful and thorough review of our work.*

## REFERENCES

- Asplund, M., Grevesse, N., Sauval, A. J., & Scott, P. 2009, *ARA&A*, 47, 481
- Berdyugina, S. V. 2005, *Living Reviews in Solar Physics*, 2, doi:10.12942/lrsp-2005-8
- Boyajian, T. S., LaCourse, D. M., Rappaport, S. A., et al. 2016, *MNRAS*, 457, 3988
- Bressan, A., Marigo, P., Girardi, L., et al. 2012, *MNRAS*, 427, 127
- Brickhouse, N. S., Cranmer, S. R., Dupree, A. K., Luna, G. J. M., & Wolk, S. 2010, *ApJ*, 710, 1835
- Casey, A. R., Ruchti, G., Masseron, T., et al. 2016, *MNRAS*, 461, 3336
- Castelli, F., & Kurucz, R. L. 2003, in *IAU Symposium*, Vol. 210, *Modelling of Stellar Atmospheres*, ed. N. Piskunov, W. W. Weiss, & D. F. Gray, A20
- Collins, K. A., Kielkopf, J. F., Stassun, K. G., & Hessman, F. V. 2017, *AJ*, 153, 77
- de Wit, W. J., Grinin, V. P., Potravnov, I. S., et al. 2013, *A&A*, 553, L1
- Foster, A. R., Ji, L., Smith, R. K., & Brickhouse, N. S. 2012, *ApJ*, 756, 128
- Gingerich, L., Knapp, T., Punzi, K., et al. 2017, in *American Astronomical Society Meeting Abstracts*, Vol. 229, *American Astronomical Society Meeting Abstracts*, 154.22
- Gondoin, P. 2003a, *A&A*, 409, 263
- . 2003b, *A&A*, 404, 355



—. 2003c, *A&A*, 400, 249

—. 2005, *A&A*, 444, 531

Grinin, V. P., Potravnov, I. S., Ilyin, I. V., & Shulman, S. G. 2015, *Astronomy Letters*, 41, 407

Grinin, V. P., Potravnov, I. S., & Musaev, F. A. 2010, *A&A*, 524, A8

Gustafsson, B., Edvardsson, B., Eriksson, K., et al. 2008, *A&A*, 486, 951

Herbig, G. H. 1960, *ApJ*, 131, 632

Herbst, W., Herbst, D. K., Grossman, E. J., & Weinstein, D. 1994, *AJ*, 108, 1906

Jacoby, G. H., Hunter, D. A., & Christian, C. A. 1984, *ApJS*, 56, 257

Jansen, F., Lumb, D., Altieri, B., et al. 2001, *A&A*, 365, L1

Kaminskii, B. M., Kovalchuk, G. U., & Pugach, A. F. 2000, *Astronomy Reports*, 44, 611

Kastner, J. H., Huenemoerder, D. P., Schulz, N. S., Canizares, C. R., & Weintraub, D. A. 2002, *ApJ*, 567, 434

Kastner, J. H., Montez, Jr., R., Rodriguez, D., et al. 2010, *ApJ*, 719, L65

Kastner, J. H., Zuckerman, B., & Forveille, T. 2008, *A&A*, 486, 239

Kennedy, G. M., Kenworthy, M. A., Pepper, J., et al. 2017, *Royal Society Open Science*, 4, 160652

- Mamajek, E. E. 2009, in American Institute of Physics Conference Series, Vol. 1158, American Institute of Physics Conference Series, ed. T. Usuda, M. Tamura, & M. Ishii, 3–10
- Mamajek, E. E. 2016, in IAU Symposium, Vol. 314, Young Stars & Planets Near the Sun, ed. J. H. Kastner, B. Stelzer, & S. A. Metchev, 21–26
- Marcy, G. W., Duncan, D. K., & Cohen, R. D. 1985, *ApJ*, 288, 259
- Melis, C., Gielen, C., Chen, C. H., et al. 2010, *ApJ*, 724, 470
- Melis, C., Zuckerman, B., Rhee, J. H., et al. 2012, *Nature*, 487, 74
- Melis, C., Zuckerman, B., Song, I., Rhee, J. H., & Metchev, S. 2009, *ApJ*, 696, 1964
- Melis, C. A. 2009, PhD thesis, University of California, Los Angeles
- Mentuch, E., Brandeker, A., van Kerkwijk, M. H., Jayawardhana, R., & Hauschildt, P. H. 2008, *ApJ*, 689, 1127
- Morrison, R., & McCammon, D. 1983, *ApJ*, 270, 119
- Neslušan, L., & Budaj, J. 2017, *A&A*, 600, A86
- Nidever, D. L., Marcy, G. W., Butler, R. P., Fischer, D. A., & Vogt, S. S. 2002, *ApJS*, 141, 503
- Pakhomov, Y. V., & Zhao, G. 2013, *AJ*, 146, 97
- Pecaut, M. J., & Mamajek, E. E. 2013, *ApJS*, 208, 9

- Potravnov, I. S., Gorynya, N. A., Grinin, V. P., & Minikulov, N. K. 2014a, *Astrophysics*, 57, 491
- Potravnov, I. S., & Grinin, V. P. 2013, *Astronomy Letters*, 39, 776
- Potravnov, I. S., Grinin, V. P., Ilyin, I. V., & Shakhovskoy, D. N. 2014b, *A&A*, 563, A139
- Potravnov, I. S., Mkrtychian, D. E., Grinin, V. P., Ilyin, I. V., & Shakhovskoy, D. N. 2017, *A&A*, 599, A60
- Randich, S., Pallavicini, R., Meola, G., Stauffer, J. R., & Balachandran, S. C. 2001, *A&A*, 372, 862
- Randich, S., Schmitt, J. H. M. M., Prosser, C. F., & Stauffer, J. R. 1995, *A&A*, 300, 134
- Rappaport, S., Gary, B. L., Kaye, T., et al. 2016, *MNRAS*, 458, 3904
- Reddy, B. E., Lambert, D. L., Laws, C., Gonzalez, G., & Covey, K. 2002, *MNRAS*, 335, 1005
- Rieke, G. H., & Lebofsky, M. J. 1985, *ApJ*, 288, 618
- Ryter, C. E. 1996, *Ap&SS*, 236, 285
- Sandquist, E. L., Dokter, J. J., Lin, D. N. C., & Mardling, R. A. 2002, *ApJ*, 572, 1012
- Schisano, E., Covino, E., Alcalá, J. M., et al. 2009, *A&A*, 501, 1013

- Sheinis, A. I., Bolte, M., Epps, H. W., et al. 2002, *PASP*, 114, 851
- Shevchenko, V. S., Vitrichenko, E. A., Grankin, K. N., Ibragimov, M. A., & Mel’Nikov, S. Y. 1993, *Astronomy Letters*, 19, 125
- Skinner, S. L., & Güdel, M. 2013, *ApJ*, 765, 3
- Snedden, C. 1973, *ApJ*, 184, 839
- Soderblom, D. R., Jones, B. F., Balachandran, S., et al. 1993, *AJ*, 106, 1059
- Spina, L., Randich, S., Palla, F., et al. 2014, *A&A*, 567, A55
- Stauffer, J. R., Hartmann, L. W., & Jones, B. F. 1989, *ApJ*, 346, 160
- Stauffer, J. R., Hartmann, L. W., Prosser, C. F., et al. 1997, *ApJ*, 479, 776
- Stephenson, C. B. 1986, *ApJ*, 300, 779
- Strüder, L., Briel, U., Dennerl, K., et al. 2001, *A&A*, 365, L18
- Turner, M. J. L., Abbey, A., Arnaud, M., et al. 2001, *A&A*, 365, L27
- Valenti, J. A., & Piskunov, N. 1996, *A&AS*, 118, 595
- Vanderburg, A., Johnson, J. A., Rappaport, S., et al. 2015, *Nature*, 526, 546
- Vogt, S. S. 1987, *PASP*, 99, 1214
- Vogt, S. S., Allen, S. L., Bigelow, B. C., et al. 1994, in *Proc. SPIE*, Vol. 2198, Instrumentation in Astronomy VIII, ed. D. L. Crawford & E. R. Craine, 362
- Vuong, M. H., Montmerle, T., Grosso, N., et al. 2003, *A&A*, 408, 581

Xu, S., Jura, M., Dufour, P., & Zuckerman, B. 2016, *ApJ*, 816, L22

Yong, D., Roederer, I. U., Grundahl, F., et al. 2014, *MNRAS*, 441, 3396

Zuckerman, B., Fekel, F. C., Williamson, M. H., Henry, G. W., & Munro, M. P.  
2008a, *ApJ*, 688, 1345

Zuckerman, B., Melis, C., Rhee, J. H., Schneider, A., & Song, I. 2012, *ApJ*, 752, 58

Zuckerman, B., & Song, I. 2004, *ARA&A*, 42, 685

Zuckerman, B., Melis, C., Song, I., et al. 2008b, *ApJ*, 683, 1085

Table 1. XMM-NEWTON X-RAY OBSERVATIONS

Detector	Useful Exposure Time (ks)	Count Rate (cts s <sup>-1</sup> )
pn	19.71	$(8.3 \pm 0.2) \times 10^{-2}$
MOS1	19.15	$(2.1 \pm 0.1) \times 10^{-2}$
MOS2	19.16	$(2.0 \pm 0.1) \times 10^{-2}$

Table 2. XMM-NEWTON OPTICAL MONITOR OBSERVATIONS

Filter	Wavelength (nm)	Date	Start Time (UT)	Magnitude (mag)	Mean Magnitude (mag)
V	543	2015-01-02	14:38:22	11.52 (0.02)	11.514 (0.008)
		2015-01-02	15:03:44	11.52 (0.03)	
		2015-01-02	15:29:06	11.51 (0.01)	
		2015-01-02	15:54:28	11.54 (0.02)	
		2015-01-02	16:19:49	11.51 (0.01)	
U	344	2015-01-02	17:15:10	12.368 (0.007)	12.371 (0.004)
		2015-01-02	17:40:32	12.38 (0.01)	
		2015-01-02	18:05:54	12.366 (0.006)	
		2015-01-02	18:31:16	12.38 (0.01)	
		2015-01-02	18:56:38	12.371 (0.007)	
B	450	2015-01-02	19:21:57	12.38 (0.05)	12.4 (0.1)
		2015-01-02	19:47:20	12.0 (0.8)	
		2015-01-02	20:12:42	12.38 (0.04)	
		2015-01-02	21:03:25	12.39 (0.01)	
UVM2	231	2015-01-02	21:28:45	15.20 (0.03)	
		2015-01-02	22:39:06	15.20 (0.03)	
		2015-01-02	23:19:27	15.16 (0.03)	
		2015-01-02	23:59:48	15.22 (0.03)	

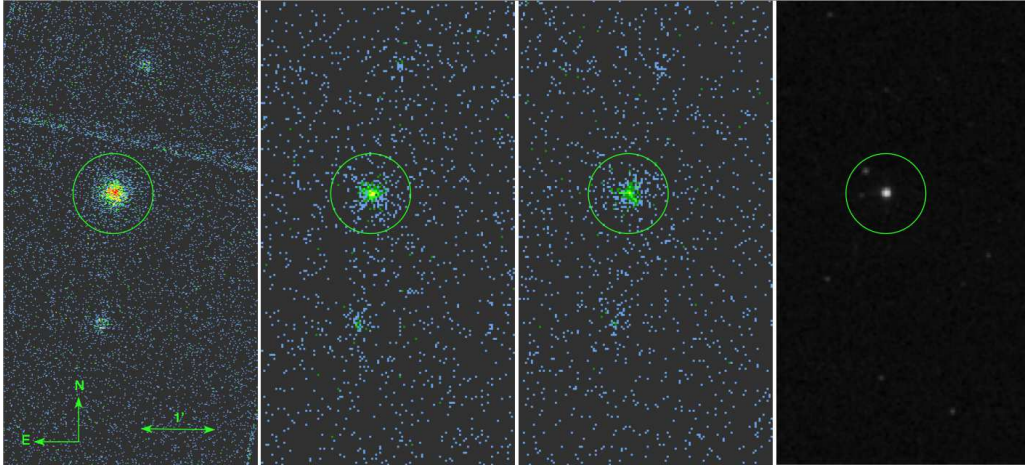


Fig. 1.— *XMM-Newton* pn (left), MOS1 (middle left), and MOS2 (middle right) images of RZ Psc, with orientation and scale indicated, alongside 2MASS J band image (right) at the same orientation and scale.

Table 2—Continued

Filter	Wavelength (nm)	Date	Start Time (UT)	Magnitude (mag)	Mean Magnitude (mag)
		2015-01-03	00:40:09	15.20 (0.03)	15.20 (0.01)



Table 3. Spectroscopic Observations Summary

Object	UT Date	Instrument	Setup	Coverage ( $\text{\AA}$ )	Resolution <sup>a</sup>	S/N <sup>b</sup>
RZ Psc	14 Aug 2013	Hamilton	640 $\mu\text{m}$ slit, Dewar #4	3850-6920	62,000	60
RZ Psc	15 Oct 2013	Hamilton	640 $\mu\text{m}$ slit, Dewar #4	3850-6920	62,000	50
RZ Psc	16 Oct 2013	Hamilton	640 $\mu\text{m}$ slit, Dewar #4	3850-6920	62,000	50
RZ Psc	21 Oct 2013	HIRES	Red Collimator	4360-8770	40,000	100
RZ Psc	13 Nov 2013	Hamilton	640 $\mu\text{m}$ slit, Dewar #4	3850-6920	62,000	30
RZ Psc	14 Nov 2013	Hamilton	640 $\mu\text{m}$ slit, Dewar #4	3850-6920	62,000	35
RZ Psc	16 Nov 2013 <sup>c</sup>	HIRES	Red Collimator	4360-8770	40,000	100,65,40 <sup>c</sup>
RZ Psc	21 Dec 2013	Hamilton	640 $\mu\text{m}$ slit, Dewar #4	3850-6920	62,000	40
RZ Psc	22 Dec 2013	Hamilton	640 $\mu\text{m}$ slit, Dewar #4	3850-6920	62,000	50
RZ Psc	03 Jan 2014	Hamilton	640 $\mu\text{m}$ slit, Dewar #4	3850-6920	62,000	60
RZ Psc	21 Jan 2014	Hamilton	640 $\mu\text{m}$ slit, Dewar #4	3850-6920	62,000	50
RZ Psc	22 Jan 2014	Hamilton	640 $\mu\text{m}$ slit, Dewar #4	3850-6920	62,000	40
RZ Psc	24 Feb 2014	Hamilton	640 $\mu\text{m}$ slit, Dewar #4	3850-6920	62,000	65
RZ Psc	28 Aug 2015	Hamilton	640 $\mu\text{m}$ slit, Dewar #4	3850-6920	62,000	65

Table 3—Continued

Object	UT Date	Instrument	Setup	Coverage ( $\text{\AA}$ )	Resolution <sup>a</sup>	S/N <sup>b</sup>
RZ Psc	10 Aug 2016	Hamilton	640 $\mu\text{m}$ slit, Dewar #4	3850-6920	62,000	100
J0109+2758	18 Nov 2016	ESI	1.0'' slit	3900-10250	4000	60
RZ Psc	28 Dec 2016	Hamilton	640 $\mu\text{m}$ slit, Dewar #4	3850-6920	62,000	35

<sup>a</sup>Resolution is measured from the FWHM of single arclines in our comparison spectra.

<sup>b</sup>S/N measurement is made at 6600  $\text{\AA}$  in the spectrum.

<sup>c</sup>Three separate spectra were obtained over the course of the night. The S/N values quoted are for each of the three spectra.

Table 4. CHARACTERISTICS OF RZ PSC FROM THE LITERATURE

Parameter	Value	Reference <sup>a</sup>
galactic latitude	-35°	
proper motion (mas/yr)	25.4, -11.9	1
proper motion error (mas/yr)	2.1, 2.0	1
$T_{eff}$ (K)	5250	2
	5350±150	3
$\log g$ (cgs)	3.41 ± 0.02	2
	4.2 ± 0.2	3
$[m/H]^b$	-0.3 ± 0.05	3
$v \sin i$ (km s <sup>-1</sup> )	23 ± 1	2
	12.0±0.5	3
RV (km s <sup>-1</sup> )	-2 ± 1.5	4, 5
	-1.2 ± 0.33	6
	-11.75±1.1	2
$v_T$ (km s <sup>-1</sup> )	2.0 ± 0.5	2
	1.0	3
$T_{dust}$ (K)	500	4
$A_V$	0.30 ± 0.05	8
Li 6708 Å, EW (mÅ)	202 ± 10	7

Table 4—Continued

Parameter	Value	Reference <sup>a</sup>
H $\alpha$ EW ( $\text{\AA}$ )	0.5	8
$L_{IR}/L_{bol}$	0.08	4
$R_*/R_\odot$	0.9	8
$M_*/M_\odot$	1.0	8
$L_*/L_\odot$	0.7	8
$\dot{M}$ ( $M_\odot\text{yr}^{-1}$ )	$\leq 7 \times 10^{-12}$	8

<sup>a</sup>References: (1) Tycho2 catalog; (2) Kaminskii et al. 2000; (3) Potravnov et al. 2014b; (4) de Wit et al. 2013; (5) Shevchenko et al. 1993; (6) Potravnov et al. 2014a; (7) Grinin et al. 2010; (8) Potravnov et al. 2017

<sup>b</sup> $[m/H] = \log(N_m/N_H)_{\text{star}} - \log(N_m/N_H)_{\text{Sun}}$  for element m compared to hydrogen; that is, the enhancement or deficiency of an element compared to the Sun.

Table 5. DERIVED CHARACTERISTICS OF RZ PSC

Parameter	Value
$T_{eff}$ (K)	$5600 \pm 75$
$\log g$ (cgs)	$4.35 \pm 0.10$
$[Fe/H]$	$-0.11 \pm 0.03$
RV (km s <sup>-1</sup> )	see Table 7
$v_T$ (km s <sup>-1</sup> )	$2.0 \pm 0.2$
Li 6708 Å, EW (mÅ)	$207 \pm 6$
A(Li)	3.05
$\log(L_X/L_{bol})$	-3.7 to -3.2
$N_H$ (cm <sup>-2</sup> )	$\sim (0.39 - 1.83) \times 10^{21}$
$A_V$	$\sim 0.66$
Spectral Type	G4
$L_*/L_\odot$	$\sim 0.6$

Table 6. Abundances of the Elements in RZ Psc

Species	Sun	RZ Psc	RZ Psc		Number of
Species	A	A	[m/H]	$\sigma$	Lines
Na I	6.14	6.18	0.04	0.09	4
Mg I	7.5	7.43	-0.07	0.09	2
Al I	6.35	6.42	0.07	0.14	3
Si I	7.41	7.53	0.12	0.05	14
Ca I	6.24	6.33	0.09	0.07	14
Sc II	3.05	2.94	-0.11	0.09	6
Ti I	4.85	4.81	0.14	0.08	25
Ti II	4.85	4.99	-0.05	0.10	3
V I	3.83	3.99	0.16	0.08	11
Cr I	5.54	5.78	0.24	0.12	5
Mn I	5.33	5.46	0.13	0.08	3
Fe I	7.50	7.40	-0.10	0.06	101
Fe II	7.50	7.41	-0.09	0.07	13
Co I	4.89	4.93	0.04	0.15	4
Ni I	6.12	6.09	-0.03	0.06	21

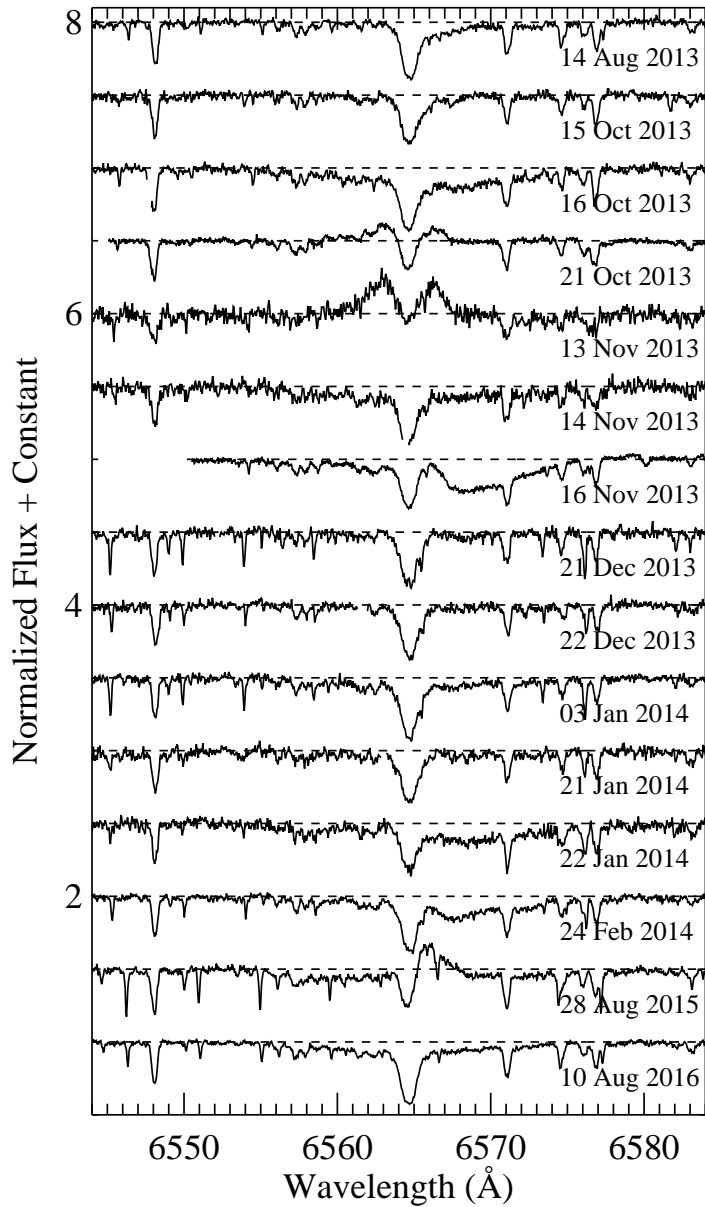


Fig. 2.— Keck HIRES and Lick Hamilton spectra of RZ Psc showing the H $\alpha$  complex and surrounding region. All spectra are continuum-fit such that the continuum has a value of unity, then shifted vertically by a constant value for clarity. The dashed line for each epoch denotes the expected continuum value. Wavelengths in this figure are plotted in vacuum. The wavelength scale for each spectrum is shifted to match the 16 Nov 2013 epoch for clarity. Some cosmic rays and bad pixels have been removed manually from the spectra.

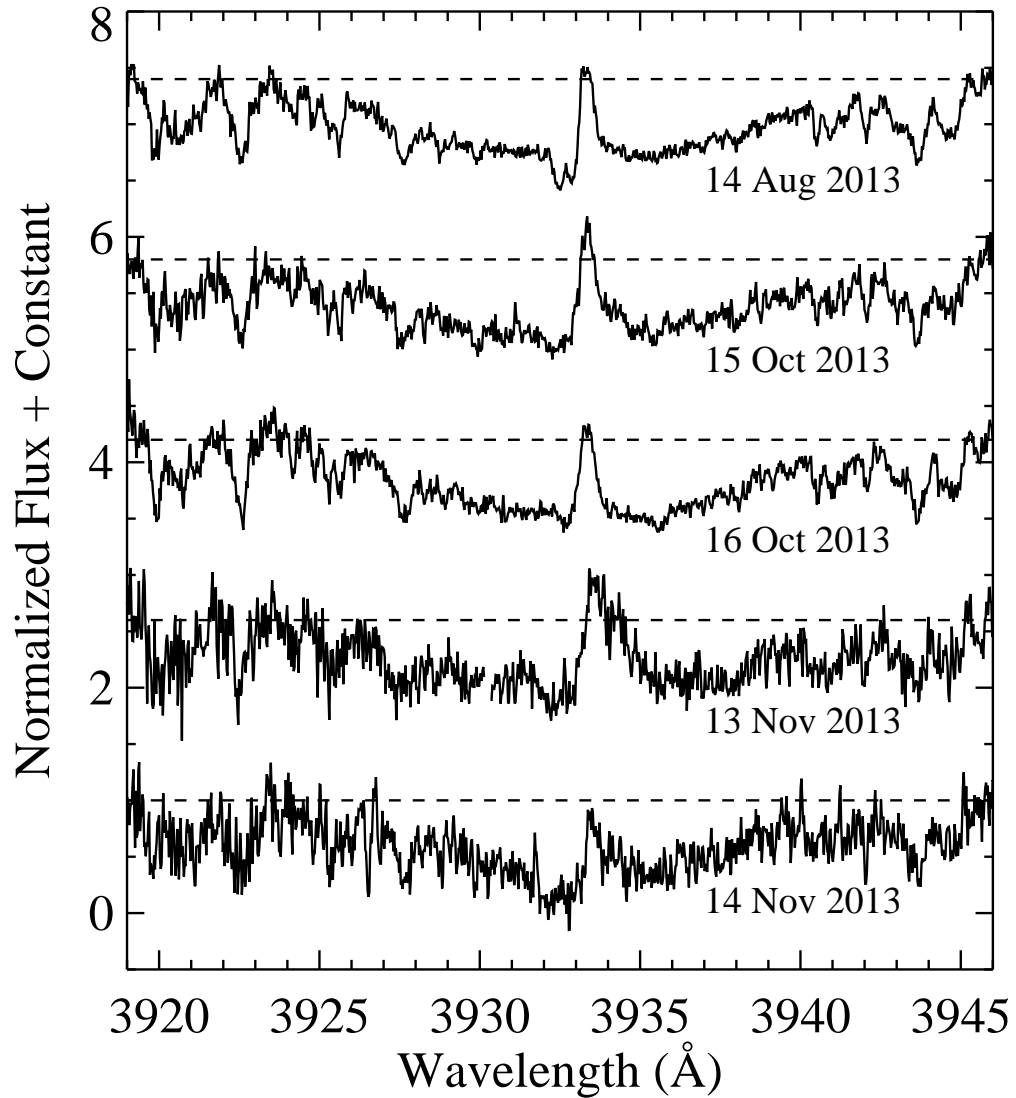


Fig. 3.— Lick Hamilton spectra of RZ Psc showing the region around the Ca II K line. The Ca II H line is essentially identical in appearance for each epoch and thus not plotted here. For each spectrum the blaze function is removed, then the spectrum is normalized to the flux level at  $\approx 3946$  Å. The dashed line indicates this normalization level and can be used as a guide for changes in the core reversal emission level. Variability in the core reversal emission and blueshifted absorption components is evident. Wavelengths in this figure are plotted in air. The wavelength scale for each spectrum is shifted to match the 14 Aug 2013 epoch for clarity. Some cosmic rays have been manually removed from the spectra.



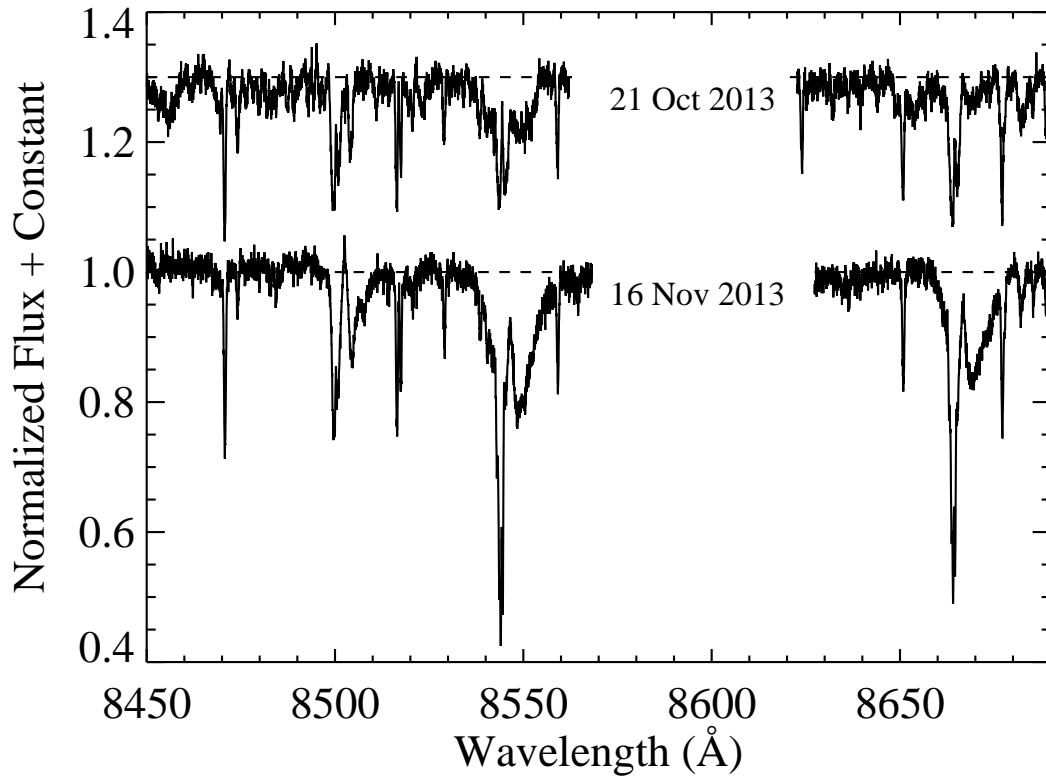


Fig. 4.— Keck HIRES spectra of RZ Psc showing the Ca II infrared triplet complex. Normalization and vertical shifting of spectra is performed as described in the caption to Figure 2. Line variability is evident, with broad absorption components and core reversal emission. Spectra from 16 Nov 2013 taken later in the night are consistent with what is shown here to within their respective S/N. Wavelengths in this figure are plotted in vacuum. The wavelength scale of the spectra are not shifted in this figure. The lack of data around 8600 Å is due to the gap between red orders for the HIRES setup used.

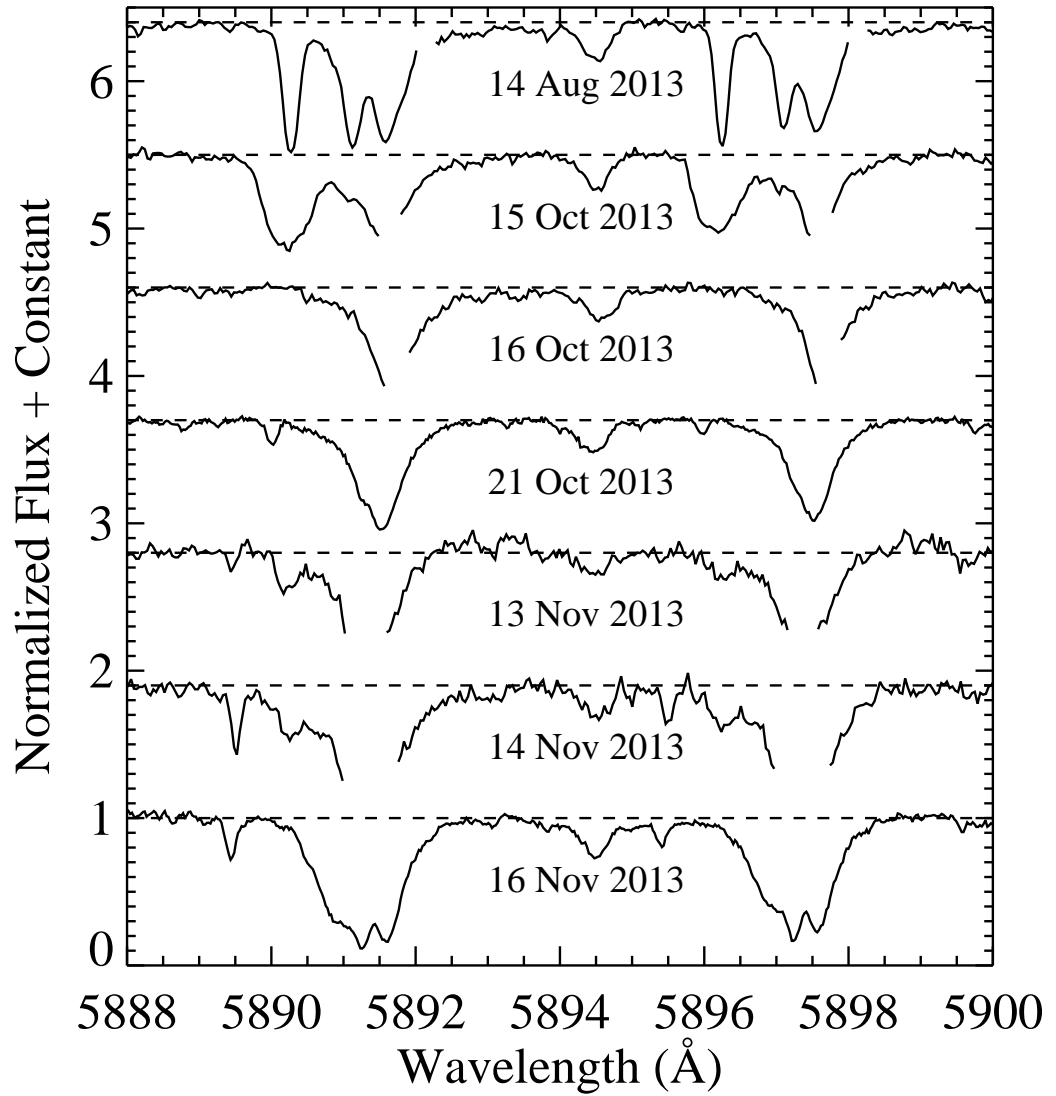


Fig. 5.— Keck HIRES and Lick Hamilton spectra of RZ Psc showing the Na D doublet complex. Normalization and vertical shifting of spectra is performed as described in the caption to Figure 2. Wavelengths in this figure are plotted in vacuum. The wavelength scale for each spectrum is shifted to match the 16 Nov 2013 epoch for clarity. In each Hamilton spectrum Na D telluric emission from nearby San Jose, CA is removed.

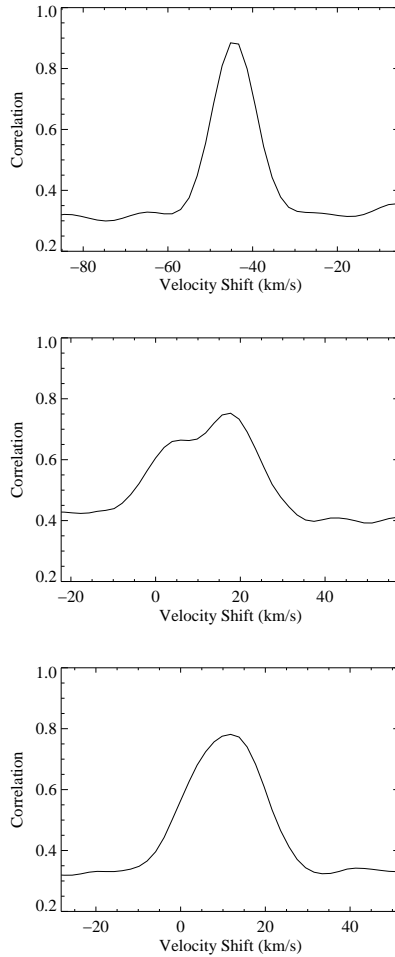


Fig. 6.— Cross-correlation spectra between Lick Hamilton observations of RZ Psc and radial velocity standard stars chosen from Nidever et al. (2002). Heliocentric velocity corrections have not been applied to any of the spectra. Wavelengths between 4800 and 4857 Å are used for the cross-correlation in each panel. *Top panel:* Cross-correlation between the bright standards HR 124 and HR 4027 using spectra from the night of UT 13 Nov 2013. A single, narrow cross-correlation peak is evident. *Middle panel:* Cross-correlation between RZ Psc and HR 4027 using spectra from the night of UT 13 Nov 2013. A double-peaked cross-correlation peak is evident. Similar cross-correlation peak shapes are recovered when using different echelle orders. *Bottom panel:* Cross-correlation between RZ Psc and HR 4027 using spectra from the night of UT 14 Nov 2013. A single cross-correlation peak is recovered, a feature seen in every order of these two spectra from this night and in general when performing cross-correlations for RZ Psc on nights other than UT 13 Nov 2013.

Table 7. Radial Velocities for RZ Psc Measured From Optical Spectra

UT Date	Heliocentric Julian Date (days)	Velocity measured (km s <sup>-1</sup> )	Comparison Star <sup>a</sup>
14 Aug 2013	2456610.76855	-2.2±0.2	HR 124
15 Oct 2013	2456580.83654	+0.0±0.2	HR 124
16 Oct 2013	2456581.74535	-2.0±0.2	HR 124
21 Oct 2013	2456586.94023	+0.4±0.2	HR 8185
13 Nov 2013	2456609.76353	-9.2±0.5 <sup>b</sup>	HR 4027
13 Nov 2013	2456609.76353	+4.6±0.5 <sup>b</sup>	HR 4027
14 Nov 2013	2456610.76855	-1.8±0.2	HR 4027
16 Nov 2013	2456612.68576	-1.6±0.2	HR 8185
16 Nov 2013	2456612.81636	-1.7±0.2	HR 8185
16 Nov 2013	2456612.94820	-2.4±0.2	HR 8185
21 Dec 2013	2456647.79631	-2.0±0.2	HR 4027
22 Dec 2013	2456648.73979	-1.8±0.2	HR 4027
03 Jan 2014	2456660.73687	-1.9±0.2	HR 4027
21 Jan 2014	2456678.68097	-1.7±0.2	HR 4027
22 Jan 2014	2456679.69084	-2.0±0.2	HR 4027
24 Feb 2014	2456712.62651	-1.7±0.2	HR 4027
28 Aug 2015	2457262.90766	-2.3±0.2	HR 124
10 Aug 2016	2457610.90309	-1.9±0.2	HR 124

Table 7—Continued

UT Date	Heliocentric Julian Date (days)	Velocity measured (km s <sup>-1</sup> )	Comparison Star <sup>a</sup>
28 Dec 2016	2457750.66765	-1.9±0.2	HR 124

<sup>a</sup>HR 8185 was observed with HIRES on UT 14 Nov 2008 in a similar setup. Otherwise, comparison stars were observed in the same night as RZ Psc.

<sup>b</sup>Two peaks were found in the cross-correlation; see Section 4.3.

Table 8. RZ PSC MODEL PARAMETERS

Parameter	Free Abundance	Model	
		T Tauri Star	Evolved Giant Star
$N_H$ ( $\times 10^{21}$ cm $^{-2}$ )	$1.8 \pm 0.5$	$0.564 \pm 0.008$	$0.390 \pm 0.006$
$kT_1$ (keV)	$0.97 \pm 0.04$	$0.67 \pm 0.05$	$0.75 \pm 0.04$
He	1.0	1.0	0.3
C	$66.6 \pm 31.3$	0.45	0.3
N	1.0	0.79	0.3
O	1.0	0.43	0.3
Ne	$0.7 \pm 1.4$	0.83	1.0
Mg	1.0	0.26	0.3
Al	1.0	0.50	0.3
Si	1.0	0.31	0.3
S	1.0	0.42	0.3
Ar	1.0	0.55	0.3
Ca	1.0	0.195	0.3
Fe	$0.9 \pm 0.3$	0.195	0.3
Ne	1.0	0.195	0.3
normalization $_1$ ( $\times 10^{-5}$ )	$4.0 \pm 1.0$	$7.6 \pm 1.0$	$6.9 \pm 0.6$
$kT_2$ (keV)	$0.27 \pm 0.05$	$1.14 \pm 0.08$	$1.6 \pm 0.1$
normalization $_2$ ( $\times 10^{-5}$ )	$3.5 \pm 1.0$	$6.8 \pm 1.0$	$6.6 \pm 0.8$



Table 9. RZ PSC X-RAY SPECTRAL ANALYSIS

Parameter	Model		
	Free Abundance	T Tauri Star	Evolved Giant Star
$N_H$ ( $\times 10^{20}$ cm $^{-2}$ )	18.0 (5.0)	5.64 (0.08)	3.90 (0.06)
$kT_1$ (keV)	0.27 (0.05)	0.67 (0.05)	0.75 (0.04)
$T_1$ (MK)	3.2 (0.6)	7.7 (0.5)	8.8 (0.4)
$kT_2$ (keV)	0.97 (0.04)	1.14 (0.08)	1.6 (0.1)
$T_2$ (MK)	11.2 (0.4)	13.3 (0.9)	19.1 (1.7)
normalization $_1$ ( $\times 10^{-5}$ )	4.0 (1.0)	7.62 (0.09)	6.91 (0.07)
$EM_1$ ( $\times 10^{52}$ cm $^{-3}$ )	2.722	5.253	4.765
normalization $_2$ ( $\times 10^{-5}$ )	3.5 (1.0)	6.8 (1.0)	6.63 (0.08)
$EM_2$ ( $\times 10^{52}$ cm $^{-3}$ )	2.414	4.658	4.567
$\chi_{red}^2$	1.053	1.120	1.298
d.o.f.	118	121	121
observed flux ( $\times 10^{-13}$ ergs s $^{-1}$ cm $^{-2}$ )	1.262	1.269	1.301
intrinsic flux ( $\times 10^{-13}$ ergs s $^{-1}$ cm $^{-2}$ )	4.152	1.616	1.653
$L_X$ ( $\times 10^{30}$ ( $\frac{D}{170 \text{ pc}})^2$ ergs s $^{-1}$ )	2.862	1.114	1.139
$\log(L_X/L_{bol})$	(-3.230, -3.294)	(-3.640, -3.704)	(-3.630, -3.694)



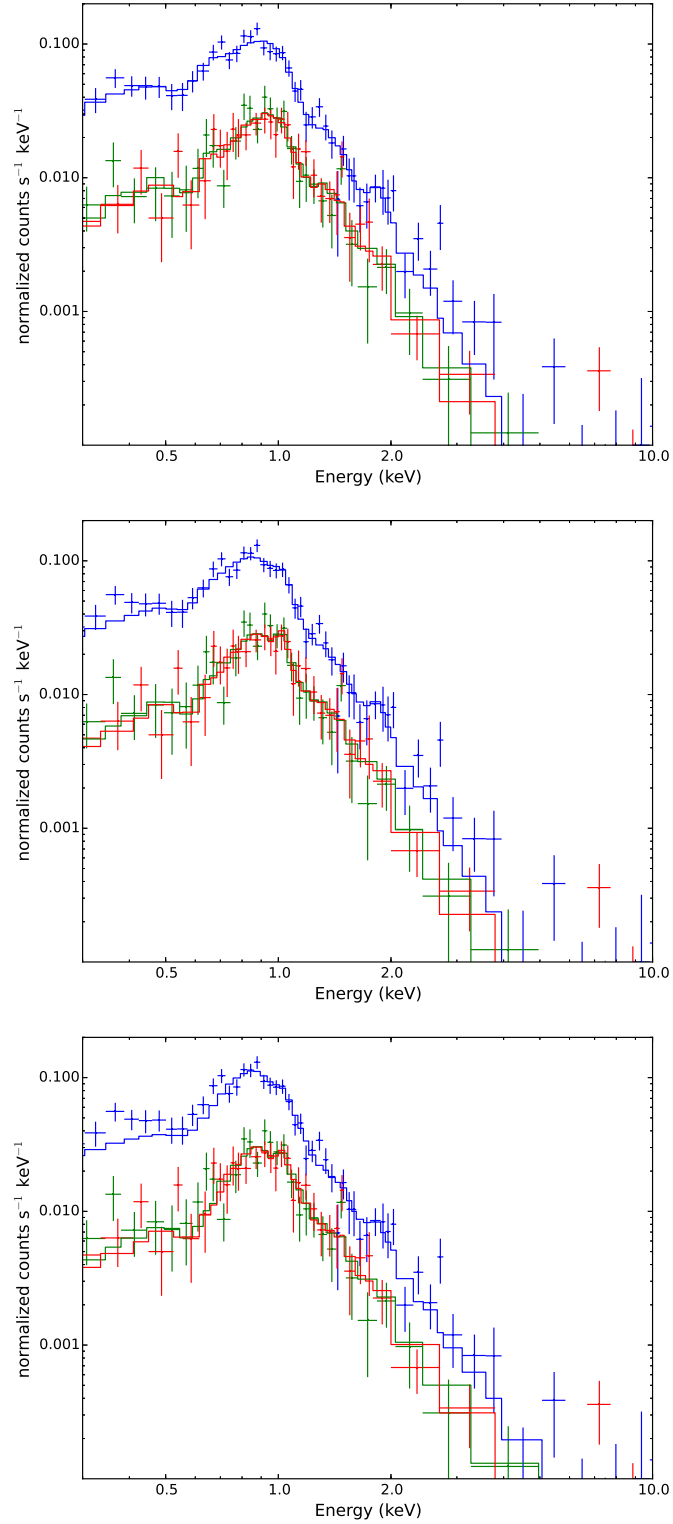


Fig. 7.— *XMM-Newton* EPIC extracted spectra (crosses) of RZ Psc for pn (blue) and MOS (red and green) detectors. Overplotted are the best-fit models (histograms): Free Abundance Model (top), T Tauri Star Model (middle), Evolved Giant Star (bottom).

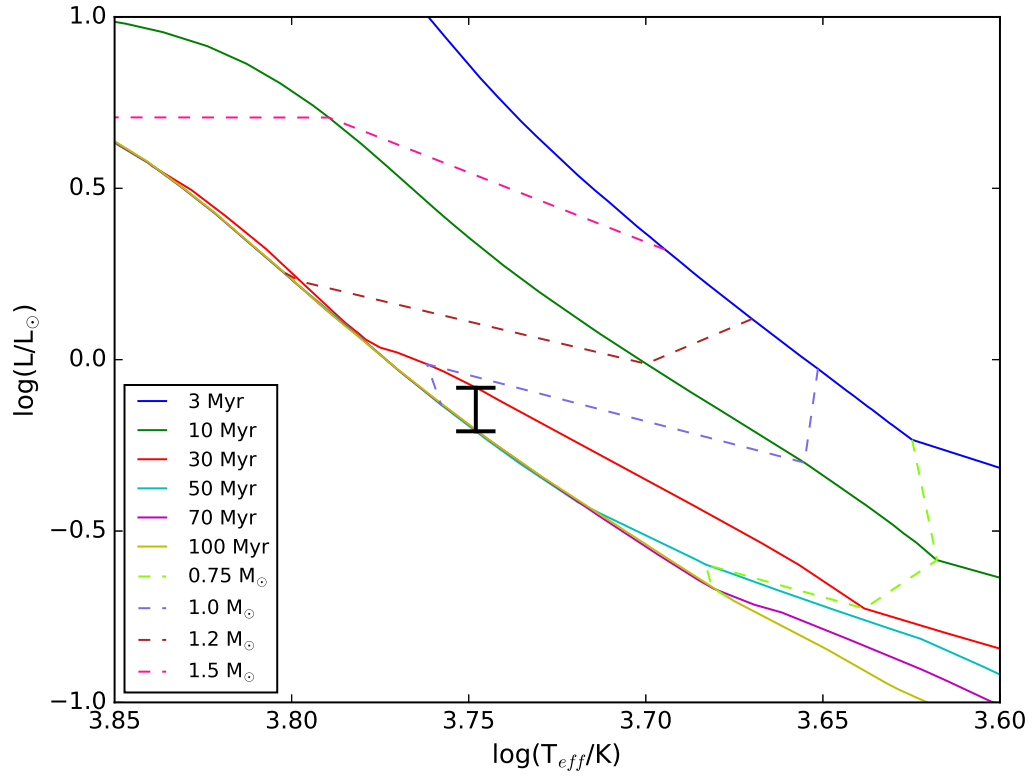


Fig. 8.— The H-R diagram position of RZ Psc, assuming an age range of 30-50 Myr, as shown by the vertical line, overlaid with PARSEC pre-main sequence isochrones and pre-main sequence tracks for a variety of masses (Bressan et al. 2012).

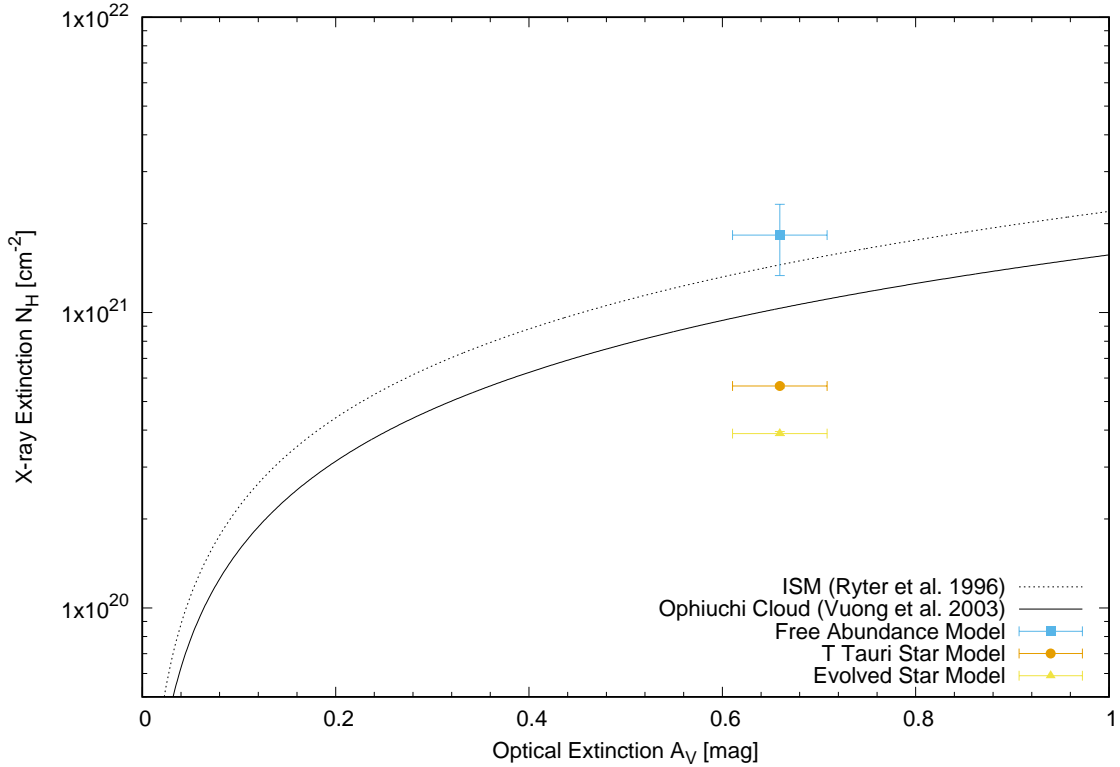


Fig. 9.— X-ray absorption column density  $N_H$  versus visual extinction  $A_V$  for RZ Psc compared to the local ISM (black dotted line; Ryter 1996) and the  $\rho$  Ophiuchi molecular cloud (black solid line; Vuong et al. 2003), where we assume  $R_V = 3.1$ . We plot the X-ray extinction values derived from spectral fitting for the derived spectral type of G4 and two different evolutionary stages (pre- and post-main sequence, respectively). The error bars represented are formal errors on the fit and do not reflect systematic uncertainties (i.e., the implicit assumption that we know all the abundances in the models).